Impact of redshift information on cosmological applications with next-generation radio surveys

Stefano Camera,[1]★ Mário G. Santos,[1]★ David J. Bacon,[2]★ Matt J. Jarvis,[3,4]
Kim McAlpine,[5] Ray P. Norris,[6] Alvise Raccanelli[7,8] and Huub Röttgering[9]

[1]*CENTRA, Instituto Superior Técnico, Universidade Técnica de Lisboa, Av. Rovisco Pais 1, 1049-001 Lisboa, Portugal*
[2]*Institute of Cosmology & Gravitation, University of Portsmouth, Dennis Sciama Building, Portsmouth P01 3FX*
[3]*Centre for Astrophysics Research, STRI, University of Hertfordshire, Hatfield AL10 9AB*
[4]*Department of Physics, University of the Western Cape, Bellville 7535, South Africa*
[5]*Department of Physics and Electronics, Rhodes University, Grahamstown 6139, South Africa*
[6]*CSIRO Astronomy & Space Science, Australia Telescope National Facility, PO Box 76, NSW 1710 Epping, Australia*
[7]*Jet Propulsion Laboratory, California Institute of Technology, Pasadena, CA 91109, USA*
[8]*California Institute of Technology, Pasadena, CA 91125, USA*
[9]*Leiden Observatory, University of Leiden, Leiden NL-2300 RA, the Netherlands*

ABSTRACT

In this paper, we explore how the forthcoming generation of large-scale radio continuum surveys, with the inclusion of some degree of redshift information, can constrain cosmological parameters. By cross-matching these radio surveys with shallow optical to near-infrared surveys, we can essentially separate the source distribution into a low- and a high-redshift sample, thus providing a constraint on the evolution of cosmological parameters such as those related to dark energy. We examine two radio surveys, the Evolutionary Map of the Universe (EMU) and the Westerbork Observations of the Deep APERTIF Northern sky (WODAN). A crucial advantage is their combined potential to provide a deep, full-sky survey. The surveys used for the cross-identifications are SkyMapper and Sloan Digital Sky Survey, for the southern and northern skies, respectively. We concentrate on the galaxy clustering angular power spectrum as our benchmark observable, and find that the possibility of including such low-redshift information yields major improvements in the determination of cosmological parameters. With this approach, and provided a good knowledge of the galaxy bias evolution, we are able to put strict constraints on the dark energy parameters, i.e. $w_0 = -0.9 \pm 0.041$ and $w_a = -0.24 \pm 0.13$, with Type Ia supernovae and cosmic microwave background priors (with a one-parameter bias in this case); this corresponds to a Figure of Merit (FoM) >600, which is twice better than what is obtained by using only the cross-identified sources and greater than four time better than the case without any redshift information at all.

Key words: cosmological parameters – cosmology: observations – large-scale structure of universe – radio continuum: galaxies.

1 INTRODUCTION

A new era for precision cosmology with radio continuum surveys is close to becoming a reality. Several experiments across the world are currently beginning operations, such as the LOw Frequency ARray[1] (LOFAR) and Apertif[2] at the Westerbork Synthesis Radio

Telescope (WSRT), in the Northern hemisphere, and the projects for the Australian[3] and African[4] SKA (Square Kilometre Array) Pathfinders, in the Southern hemisphere.

Recently, Raccanelli et al. (2012) have shown promising forecasts for constraining cosmological parameters using some of the large-scale radio continuum surveys planned for these forthcoming telescopes. In this paper, we investigate the usefulness of including redshift information for the subsample of radio continuum sources

---

★E-mail: stefano.camera@ist.utl.pt (SC); mgrsantos@ist.utl.pt (MGS); david.bacon@port.ac.uk (DJB)
[1] http://www.lofar.org
[2] http://www.astron.nl/general/apertif/apertif

[3] http://www.atnf.csiro.au/projects/askap/
[4] http://www.ska.ac.za/index.php

which are successfully cross-identified with optical surveys containing photometric or spectroscopic redshifts. We examine the impact of this partial redshift knowledge on cosmological constraints with forthcoming radio surveys. The underlying effect of this multi-wavelength information is reasonably simple to understand: shallow optical surveys should be able to identify most of the low-redshift galaxies from these large radio surveys, allowing us to 'extract' the high-redshift tail expected for the radio distribution of sources.

Although the detailed analysis is more involved, basically the combination of these two 'macro' redshift bins will give us a powerful constraint on the redshift evolution of cosmological models as an approximate alternative to demanding redshift surveys. For the purpose of this work and in order to clarify the improvements achieved with this redshift information, we will focus on the radio-galaxy two-point correlation function as the cosmological observable; there are several other available probes such as the integrated Sachs–Wolfe effect and cosmic magnification – as discussed in Raccanelli et al. (2012) – which will merit further investigation in the context of specific modified matter and gravity theories (Camera et al., in preparation).

This paper is structured as follows. We briefly present the EMU and WODAN surveys and their main characteristics in Section 2, while the surveys used for cross-identifications, providing redshift information, are described in Section 3. Section 4 outlines the data analysis procedure which we will consider for obtaining cosmological constraints. In Section 5, we give the most important formulae for the galaxy clustering angular power spectrum and its statistics. In Section 6, we introduce the fiducial dark energy (DE) model used in our analyses and in Section 7 we describe our method. In Section 8, we present the analysis of the combined radio and optical surveys for constraining the DE equation of state. First, we present the cosmological constraints available when there is no redshift information at all; secondly, we show what would be obtained in the idealized case of full knowledge of every radio-source redshift. Finally, we describe the realistic scenario expected to be available in the recent future, where we cross-identify as many EMU/WODAN galaxies as possible with optical redshift surveys, in particular SkyMapper and Sloan Digital Sky Survey (SDSS). For this last case, we scrutinize a simple one-parameter model for the radio-galaxy bias, as well as a two-parameter model which accounts for a further redshift dependence. Conclusions are drawn in Section 9.

2 FORTHCOMING RADIO SURVEYS

Here, we present the two survey designs we use in our calculations. A summary of their properties is given in Table 1, where N_g represents the total number of detected radio galaxies at 10σ and z_m the median redshift (see Raccanelli et al. 2012 for details). It is worth noticing that these two surveys have the same redshift distribution of sources, shown in Fig. 1 (black histogram). Furthermore, they will cover the entire sky, if their data are combined. This is one of the major strengths of the present analysis, providing a homoge-
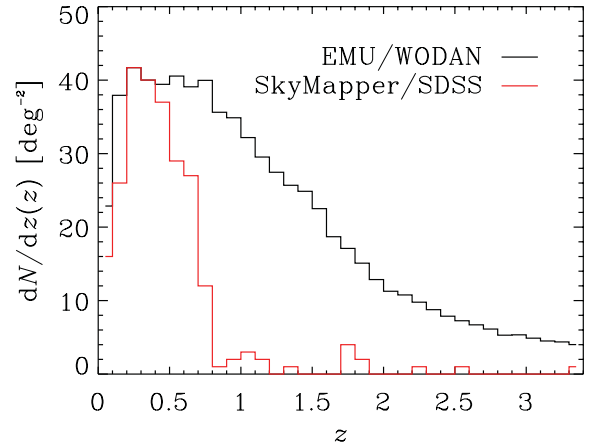
Figure 1. Redshift distribution of sources $dN/dz(z)$ for the EMU/WODAN surveys. The area is normalized to the mean galaxy number density. The red histogram shows the distribution of radio objects which have optical counterparts in SkyMapper and SDSS.

neous all-sky catalogue, since the two surveys have basically the same sensitivity, galaxy number density and redshift distribution.

2.1 EMU

Evolutionary Map of the Universe (EMU; Norris et al. 2011) is an all-sky continuum survey planned for the new Australian SKA Pathfinder (ASKAP; Johnston et al. 2008) telescope under construction on the Australian candidate SKA site in Western Australia. The primary goal of EMU is to make a deep 10 μJy beam^{-1} radio continuum survey of the entire Southern Sky, extending as far north as $+30°$ at a resolution of $\sim$10 arcsec; it will also have sensitivity to extended structures. The EMU survey is expected to begin in 2013.

2.2 WODAN

Westerbork Observations of the Deep APERTIF Northern sky (WODAN) survey is planned to chart the entire northern sky above $+30°$ down to a proposed rms flux density at 1.4 GHz of 10 μJy per beam with a resolution of $\sim$15 arcsec (Rottgering et al. 2011). It will be able to do this because of the new phased array feeds (APERTIF) being put on the WSRT (Oosterloo, Verheijen & van Cappellen 2010). The current schedule for the commencement of APERTIF surveys is 2013.

LOFAR is another experiment which merits comment. This is a multi-national telescope with stations spanning Europe; the core of LOFAR is situated in the north-east of the Netherlands, with stations on longer baselines both within the Netherlands and across Germany, UK, France and Sweden. Other stations may be added throughout the rest of Europe in the coming years. LOFAR large-area continuum surveys probe to similar depth and source densities as EMU and WODAN (Rottgering 2003; Rottgering et al. 2011; van Haarlem et al., in preparation), and can therefore be used on their own or in conjunction with EMU and WODAN for cosmological studies. This is because the lower frequency of LOFAR makes it sensitive to different source populations and provides spectral information. However, for the rest of this paper we concentrate on only the EMU and WODAN surveys, noting that LOFAR could also be used in the Northern hemisphere.

Table 1. Specifics of the EMU and WODAN surveys, where N_g is the total number of detected sources at 10σ, and z_m the median redshift.

Survey	Area	Frequency	Sensitivity	N_g	z_m
EMU	3π	1400 MHz	10 μJy	2.2×10^7	1.1
WODAN	π	1400 MHz	10 μJy	7.3×10^6	1.1

3 SURVEYS FOR CROSS-IDENTIFICATIONS

In this section, we present the surveys we shall use to cross-identify the EMU/WODAN sources. Our goal is to obtain any sort of redshift information for some of the radio sources that will be detected by the EMU and WODAN surveys using surveys available around the same time. We shall mainly focus on current and forthcoming large-scale surveys which have multi-filter data across the optical and near-infrared to facilitate reasonably accurate photometric redshifts, either through pure template fitting methods (e.g. Benitez 2000; Bolzonella, Miralles & Pello' 2000), template fitting methods combined with known spectroscopic redshifts (e.g. Feldmann et al. 2006; Ilbert et al. 2006; Salvato et al. 2011) or with empirical methods, such as artificial neural networks (e.g. Firth, Lahav & Somerville 2003; Collister & Lahav 2004) or Gaussian Processes (e.g. Way & Srivastava 2006; Bonfield et al. 2010).

The most important surveys to consider for these radio surveys are therefore SkyMapper (Keller et al. 2007) and SDSS (Eisenstein et al. 2011) at optical wavelengths, combined with the UKIRT (United Kingdom Infrared Telescope) Infrared Deep Sky Survey Large Area Survey (UKIDSS-LAS; Lawrence et al. 2007) and the proposed UKIRT Hemisphere Survey at northern latitudes, along the VISTA (Visible and Infrared Survey Telescope for Astronomy) Hemisphere Survey at southern latitudes. We also note that the Wide-field Infrared Survey Explorer (WISE; Wright et al. 2010) could also play a role in helping with photometric redshifts over both hemispheres. Further in the future, there are deeper planned surveys observing large areas, such as those using the Large Synoptic Survey Telescope (LSST; Ivezic et al. 2008) and Euclid[5] (Laureijs et al. 2011). We do not consider the slightly smaller area surveys such as the Dark Energy Survey (DES; Abbott et al. 2005) in this paper, but note that they could provide important additional information by constraining redshifts to fainter magnitudes and higher redshifts.

In this paper, we focus on SkyMapper and SDSS. The former is a $20\,000\,\mathrm{deg}^2$ optical survey of the southern sky, whilst the latter will cover $12\,000\,\mathrm{deg}^2$ in the northern sky. For both surveys, we adopt a conservative magnitude limit of $r < 22$ mag which should ensure that the redshifts can be measured to reasonable accuracy and certainly to the level required for our investigations here. SkyMapper should provide photometric redshifts whilst SDSS should be able to also provide spectroscopic redshifts – at least for low redshifts.

To assess the number of radio sources in both WODAN and EMU that will have an optical counterpart to $r \sim 22$, we use the recent results of McAlpine et al. (2012), who analysed how many reliable cross-identifications to radio sources can be found as a function of resolution and depth of the radio data coupled with the depth of the optical and near-infrared data using the VISTA Deep Extragalactic Observaitions (VIDEO) Survey (Jarvis et al. 2012). In Fig. 1 we show the expected redshift distribution of radio sources detected at $>10\sigma$ in EMU and WODAN (black) along with the expected number of optical counterparts at $r < 22$ from SDSS and SkyMapper (red).

4 STRATEGY FOR REDSHIFT BINNING

In this section, we describe a realistic scenario for an analysis leading to cosmological constraints including redshift information. First, we note that the redshift distribution shown in Fig. 1 should be known with reasonable accuracy for forthcoming radio surveys.

Table 2. Adopted bins for cross-identifications with SkyMapper and SDSS (equal sized bins for each range). The assumed scatter for photo-z bins is $0.05(1 + z)$ for photo-z.

	SkyMapper	SDSS
Spectroscopic	–	3 bins ($0.0 < z < 0.3$)
Photometric	5 bins ($0.0 < z < 0.8$)	3 bins ($0.3 < z \lesssim 0.8$)

This is because there are radio surveys such as the Australia Telescope Large Area Survey (ATLAS; Norris et al. 2006) and radio surveys covering the UKIDSS-Ultra Deep Survey (Simpson et al. 2006) and the COSMOS (Cosmological Evolution Survey) field (Schinnerer et al. 2010), covering a few square degrees to the same depth as EMU and WODAN, and for which deep spectroscopic data are becoming available. We shall consider an analysis where a fraction of the EMU/WODAN galaxies are cross-identified with SkyMapper and/or SDSS. Hence, for those sources we shall be able to perform an actual redshift binning.

We assume that spectroscopic redshifts have a negligible uncertainty, and that they will be available for the radio sources using the SDSS up to $z \simeq 0.3$. For those sources without spectroscopic redshifts, namely radio sources with identifications in SkyMapper and those without spectroscopic redshifts in SDSS (i.e. with $z > 0.3$) we shall rely on photometric redshifts and assume a photometric-redshift scatter $\sigma_z^{\mathrm{ph}} = 0.05(1 + z)$. The binning we use is summarized in Table 2. Note that this does not refer to all the sources that will be detected by these optical surveys, but only to those that are cross-matched to EMU and WODAN. In particular, radio active galactic nuclei detected in the radio occupy massive galaxies, which should correspond to the SDSS LRGs (Luminous Red Galaxies), so in principle we could have spectroscopic information from SDSS to higher redshifts (e.g. up to $z \sim 0.5$ instead of $z \lesssim 0.3$ that we assume here).

On the other hand, one of the most promising properties of EMU and WODAN is the high-redshift tail of their source distribution (see Fig. 1), which is composed of galaxies difficult to cross-identify with SkyMapper or SDSS due to their faint nature. Nevertheless, these can still bring important additional information to the analysis. We will assess the impact of these objects by making calculations for both a cross-identified catalogue, and a catalogue whose source distribution is given by the difference between the EMU/WODAN source distribution and that of the survey used for the cross-identifications. In addition, we note that the sky coverage of the optical surveys will not overlap exactly with EMU or WODAN. Therefore, we can also make calculations for a third catalogue which follows the EMU/WODAN source distribution and covers all the sky not surveyed by the optical surveys.

To summarize, the analysis for this realistic-binning strategy will combine three 'effective surveys', whose dN/d$z(z)$ are defined as follows:

(i) all the EMU/WODAN galaxies cross-identified by SkyMapper/SDSS, appropriately binned in redshift (see Table 2);

(ii) all the EMU/WODAN galaxies which are in the same patch of sky as SkyMapper/SDSS but which are not cross-identified;

(iii) the part of the EMU/WODAN survey probing the sky left uncovered by SkyMapper/SDSS.

5 GALAXY ANGULAR POWER SPECTRUM

We now introduce the main cosmological observable considered in this work. For our radio surveys, let us consider the two-point

[5] http://www.euclid-ec.org

angular correlation function ξ^g of radio sources. It can be seen as the excess probability δ_g of finding two radio sources at a certain physical separation $s = |\boldsymbol{x} - \boldsymbol{y}|$ one from each other (Peebles 1980), viz.

$$\langle \delta_g(\boldsymbol{x})\delta_g(\boldsymbol{y})\rangle \equiv \delta_D(s)\xi^g(s); \tag{1}$$

here, δ_D is Dirac's delta function. By performing the Fourier transform of such an observable we obtain the radio source overdensity power spectrum $P^g(k, z)$, where $\boldsymbol{k}$ is the physical wavenumber, with $k = |\boldsymbol{k}|$. This is related to the underlying total-matter power spectrum $P^\delta(k, z)$ of the matter density contrast $\delta \equiv \delta\rho/\rho$ by the radio-source bias function b_g, which we discuss in greater detail in Section 5.1. Thus, we have $P^g(k, z) = b_g{}^2 P^\delta(k, z)$.

However, when we have no radial information, we instead deal with projected quantities. Thus, the angular power spectrum $C^g(\ell)$ of the radio source fluctuation – where ℓ is the angular wavenumber – then reads

$$C^g(\ell) = 4\pi \int \frac{dk}{k} \left[W^g(\ell, k) \right]^2 P^g(k, z = 0), \tag{2}$$

with $W^g(\ell, k)$ a proper line-of-site weight function. A widely used simplification is given by the so-called Limber's approximation (Kaiser 1992), where $\ell = k\chi$; here, $\chi(z)$ is the radial comoving distance, which is related to the Hubble expansion rate $H(z)$ via $d\chi = dz/H(z)$. Limber's approximation is valid when $\ell \gg 1$, but it has been shown that the convergence is already good for $\ell \gtrsim 10$ (e.g. Hu 2000). Therefore, it is a suitable approximation, since for larger angular scales the cosmic variance uncertainty is dominant. In this limit we have

$$C^g(\ell) = \int d\chi \left[\frac{W^g(\chi)}{\chi} \right]^2 P^\delta \left(\frac{\ell}{\chi}, \chi \right), \tag{3}$$

with $W^g(\chi)$ defined through

$$W^g[\chi(z)] = H(z)b_g(z)\frac{dN}{dz}(z). \tag{4}$$

5.1 Radio-galaxy bias

The radio-source bias is worth a deeper digression. In this paper, we adopt the approach of Raccanelli et al. (2012). They used the simulations of Wilman et al. (2008) (see also Wilman et al. 2010) for the SKA continuum survey. By generating source catalogues with the *S*-cube data base[6] corresponding to the radio flux-density limits of the proposed EMU and WODAN surveys, they obtained an estimate of the bias for each source population used here. Note that the source distribution and bias of Wilman et al. (2008) are compatible with several observational results such as the NVSS survey (Condon et al. 1998). In Fig. 2, we show the product of the bias and the redshift distribution of the sources, i.e. $W_g(z)/H(z)$; we also illustrate the products of the bias and redshift distribution for surveys at 1 mJy, 5 mJy and 10 mJy to illustrate the advance that is expected from the new generation of radio surveys compared to surveys such as the NVSS.

In this paper, we assume a reasonable knowledge a priori of the bias evolution, so that only a one- and a two-parameter model are used, as explained below. The analysis of small sky patches with deep radio data and detailed redshift information from other multi-wavelength data should provide a reasonable measurement of the
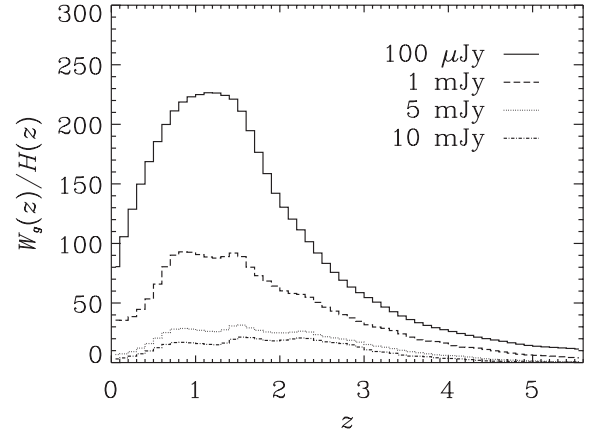
Figure 2. The bias multiplied by the redshift distribution of the radio sources as a function of redshift for the EMU and WODAN surveys (solid line). Also shown are the product of the bias and redshift distribution for surveys at 1 mJy, 5 mJy and 10 mJy to illustrate the advance that is expected from the new generation of radio surveys compared to surveys such as the NVSS. For the functional forms of the bias of each source population, we refer to Raccanelli et al. (2012, fig. 3; see also Wilman et al. 2008).

bias directly from the redshift space distortions without assumptions on the DE model, and thus allow for this more simple parametrization (note that the bias is assumed scale independent). Nevertheless, as constraints on the DE evolution become more stringent, a more precise procedure will be required, such as a joint fit to both the bias and DE model using the deep, small survey and the large, shallow radio survey combined. Specifically, from correlation function of the faint radio sources from the deep survey, we shall have important information on the galaxy clustering as a function of redshift, whilst the data from shallow, large-scale surveys will provide information on the scale-dependent effects of DE. Moreover, this could include other estimators such as the ISW (Integrated Sachs–Wolfe) and, in particular, the cosmic magnification, which is less sensitive to the bias issue. Finally, other possible parametrizations of the bias within the theoretical framework of the halo model (e.g. Cooray & Sheth 2002, for a review) should be explored; they could allow us to reduce the number of parameters. The current paper addresses the constraining capabilities of the next generation of radio surveys that will soon be available, when combined with other multi-wavelength data using the clustering estimator as a benchmark, and we hope that the results obtained open the window for further studies.

The effective bias $b_g(z)$ of equation (4) accounts for the different biases for each source population. The main results of this work (Section 8.3) have been obtained by allowing for the amplitude of this effective bias to take any value, while maintaining the redshift evolution of Raccanelli et al. (2012, their fig. 3). That is to say, we parametrize the effective bias as $A_b b_g(z)$, with a fiducial value $A_b = 1$, and we then marginalize the whole Fisher matrix over such amplitude.

Nonetheless, we also study the effects of allowing for a greater uncertainty in the redshift evolution of the bias by introducing another parameter that accounts for an additional redshift dependence. Specifically, we make the substitution

$$A_b b_g(z) \to (A_b + B_b z) b_g(z), \tag{5}$$

with $B_b = 0$ as a fiducial value. We shall see that this will not qualitatively change our results – though the presence of one more free parameter necessarily broadens the constraints.

6 DYNAMICAL DARK ENERGY

Here, we briefly outline the cosmological model tested in our analysis. Since the objective of this work is to test the effects of redshift information, we choose a dynamical DE model as our benchmark. We consider a flat Friedmann–Lemaître–Robertson–Walker Universe, filled with a perfect fluid of baryons, cold dark matter and DE. Their abundances in units of the critical density are Ω_b, Ω_{DM} and $\Omega_{DE} = 1 - \Omega_m$, respectively, and the total matter contribution is $\Omega_m \equiv \Omega_b + \Omega_{DM}$. Therefore, the expansion history of the Universe $H \equiv d \ln a / dt$ is (see e.g. Bartelmann 2010)

$$H(z) = H_0 \sqrt{\Omega_m (1+z)^3 + \Omega_{DE} f_{DE}(z)}, \qquad (6)$$

with $H_0 = 100\, h\, \text{km s}^{-1}\, \text{Mpc}^{-1}$ the Hubble constant and $f_{DE}(z)$ the (unknown) function governing the time evolution of DE.

For an exhaustive and recent review on DE in general, we suggest to the reader the comprehensive monograph of Amendola & Tsujikawa (2010). For the purpose of this work, it is sufficient to say that, in principle, there is a time-dependent equation of state linking the DE pressure to its energy density, namely

$$p_{DE}(a) = w_{DE}(a)\rho_{DE}(a), \qquad (7)$$

where $a = 1/(1+z)$ is the scale factor. Thus, $f_{DE}(z)$ in equation (6) is

$$f_{DE}(z) = \exp\left[-3 \int_1^a da' \frac{1 + w_{DE}(a')}{a'}\right]. \qquad (8)$$

Hereafter, we shall use the well-known Chevallier–Polarski–Linder parametrization (Chevallier & Polarski 2001; Linder 2003)

$$w_{DE}(a) = w_0 + (1-a)w_a, \qquad (9)$$

which is a Taylor expansion around a cosmological constant (today). Indeed, the Λcold dark matter (ΛCDM) limit is reached when $w_0 \to -1$ and $w_a \to 0$.

To highlight why including some redshift information is important for the aim of constraining DE with the radio source angular power spectrum, in Fig. 3 we show the $C^g(\ell)$ of equation (3) for different redshift bins. Ultimately, this means that the angular power spectra can in principle probe departures from standard ΛCDM, if
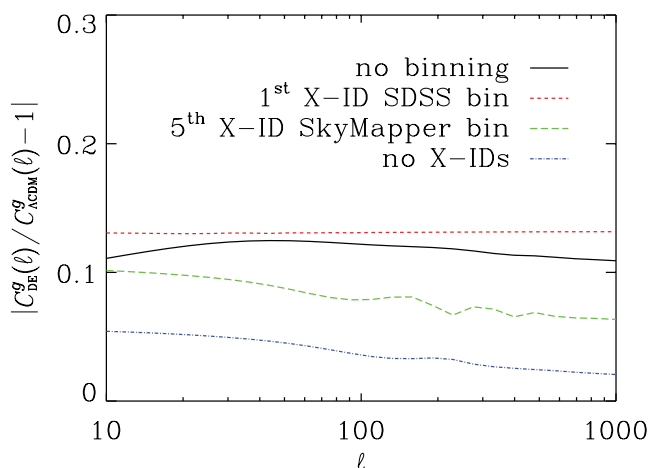
Figure 3. Relative difference between DE and ΛCDM galaxy clustering angular power spectra. The black (solid) curve refers to the unbinned EMU+WODAN case, the red (short-dashed) and the green (long-dashed) curves correspond – according to Table 2 – to the first SDSS and the last SkyMapper bin, respectively, and the blue (dot–dashed) line corresponds to the EMU/WODAN sources without cross-identifications (see Fig. 1).

the signal-to-noise ratio is sufficiently high. We plot the relative difference between the DE and ΛCDM galaxy-clustering angular power spectra as a function of the angular scale ℓ for the different effective surveys introduced in Section 4. Specifically, the solid (black) curve refers to the standard, unbinned EMU+WODAN case, while the short-dashed (red) and the long-dashed (green) curves, respectively, correspond to the first SDSS and the last SkyMapper bin (see Fig. 1 and Table 2); the dot–dashed (blue) line corresponds to the high-z tail of the effective survey (*ii*). In the next section we shall calculate the degree to which we can measure these departures from ΛCDM given realistic source densities.

7 METHOD AND FISHER MATRIX FORMALISM

The expected errors on the model parameters can be estimated via the Fisher information matrix (Fisher 1935; Jungman et al. 1996; Tegmark, Taylor & Heavens 1997). This has the advantage that different observational strategies can be analysed and this can be very valuable for experimental design. The Fisher matrix gives the best errors to expect, and is accurate if the likelihood surface near the peak is adequately approximated by a multivariate Gaussian. Hence, the Fisher matrix is simply the sum of the Fisher matrices of each ℓ mode,

$$\mathbf{F}_{\alpha\beta} = \sum_{\ell=\ell_{min}}^{\ell_{max}} \frac{2\ell+1}{2} f_{sky} \frac{\partial C^g(\ell)}{\partial \vartheta_\alpha} \left(\mathbf{C}_\ell^{g,g}\right)^{-1} \frac{\partial C^g(\ell)}{\partial \vartheta_\beta}, \qquad (10)$$

where f_{sky} is the fraction of the sky covered by the survey under analysis and $\boldsymbol{\vartheta} = \{\Omega_m, \Omega_b, w_0, w_a, h, n_s, \sigma_8, A_b\}$ is the parameter set, with A_b the overall galaxy-bias amplitude (as introduced in Section 5.1). $\mathbf{C}_\ell^{g,g}$ is the covariance for a given ℓ mode,

$$\mathbf{C}_\ell^{g,g} = \left[C^g(\ell) + \frac{1}{N_g}\right]^2, \qquad (11)$$

where the second term is related to the Poisson noise, N_g being the mean number density of sources per steradian.

We remind the reader that we are considering Limber's approximation, the sum in equation (10) therefore starts at $\ell_{min} = 10$. To check the robustness of the results obtained under such assumption, we also performed the analysis with $\ell_{min} = 2$. However, we found that the enhancements thus yielded are only of a few per cent. This is because, at such large scales, the cosmic variance heavily spoils the signal. Hence, we find it reasonable to neglect $\ell < 10$. Furthermore, Hu (2000) has shown that Limber's approximation leads to an overestimation of the signal for $\ell \lesssim 10$, which means that the actual improvement in the analysis would be even smaller than what we have estimated. On the other hand, $\ell_{max} = 1000$ is kept fixed.

At this stage, the overall galaxy-bias amplitude A_b represents a 'nuisance' parameter, since this quantity is not one of the fundamental cosmological parameters that we want to constrain. This results in a general broadening of all the marginal errors, particularly of the power-spectrum normalization σ_8, which is completely degenerate with the bias amplitude. Therefore, we marginalize over both these parameters (Wang 2008). To avoid any possible numerical instability in the marginalizing procedure, we calculate the Fisher matrix marginalized over σ_8 and A_b as (Albrecht et al. 2009)

$$\mathbf{G} = \mathbf{F}^{\varphi\varphi} - \mathbf{F}^{\varphi\psi}\mathbf{U}\boldsymbol{\Lambda}^{-1}\mathbf{U}^T\mathbf{F}^{\varphi\psi}, \qquad (12)$$

where we define $\boldsymbol{\varphi} = \{\Omega_m, \Omega_b, w_0, w_a, h, n_s\}$ and $\boldsymbol{\psi} = \{\sigma_8, A_b\}$; therefore, $\mathbf{F}^{\varphi\varphi}$ is the block of the total Fisher matrix containing the parameters we want to constrain, whilst $\mathbf{F}^{\psi\psi}$ is the nuisance-parameter Fisher sub-matrix. Here, $\boldsymbol{\Lambda}$ is the diagonal matrix whose

elements are the eigenvalues of $\mathbf{F}^{\psi\psi}$, whilst $\mathbf{U}$ is the orthogonal matrix diagonalizing $\mathbf{F}^{\psi\psi}$. By using equation (12), our marginalizing procedure is more stable, since degeneracies in $\mathbf{F}^{\varphi\varphi}$ are properly propagated to $\mathbf{G}$ with no instabilities, and we do not even worry about a possibly ill-conditioned $\mathbf{F}^{\psi\psi}$ sub-matrix, since we check its stability on the fly by the diagonalization.

Another important quantity that we calculate is the correlation between the parameter pair $\varphi_i - \varphi_j$, which is defined as[7]

$$r_{\varphi_i - \varphi_j} = \frac{\left(\mathbf{G}^{-1}\right)_{ij}}{\sqrt{\left(\mathbf{G}^{-1}\right)_{ii}\left(\mathbf{G}^{-1}\right)_{jj}}}. \tag{13}$$

This quantity tells us whether the two parameters are completely uncorrelated (if it is zero) or completely degenerate (if it is ± 1), or have some intermediate level of correlation.

Finally, we calculate the DE Figure of Merit (FoM), as introduced by the Dark Energy Task Force (Albrecht et al. 2009)

$$\text{FoM} = \frac{1}{\sqrt{\det\left[\left(\mathbf{G}^{-1}\right)_{w_0 w_a}\right]}}; \tag{14}$$

this is proportional to the inverse of the area encompassed by the ellipse representing the 68 per cent confidence level in the (w_0, w_a)-plane. Therefore, the tighter the constraints, the larger the FoM. We also combine all our results with the cosmic microwave background (CMB) Fisher matrix obtained for the *Planck* survey (Planck Collaboration 2005) and the latest measurements of Type Ia supernovae (SNeIa) from the Union2 sample (Amanullah et al. 2010).

Since one of our main goals is to show the capability of our method of discriminating between the fiducial DE model and ΛCDM, there is also another possible approach. There is a pivot redshift z_p where the uncertainty on the equation-of-state parameter is minimized for a given data model. Hence, rather than using w_0, we can introduce

$$w_p = w_0 - \frac{z_p}{1 + z_p} w_a. \tag{15}$$

It is also easy to demonstrate that $\text{FoM} = \left(\sigma_{w_p}\sigma_{w_a}\right)^{-1}$ holds (Albrecht et al. 2009).

8 CONSTRAINTS ON DARK ENERGY

In order to assess the impact of using redshift information in our analysis, we start by considering a flat Universe in the matter-dominated era with matter fraction $\Omega_m = 0.28$, baryonic contribution $\Omega_b = 0.045$, Hubble constant (in units of $100\,\text{Mpc}^{-1}$) $h = 0.7$, slope of the primordial power spectrum $n_s = 0.96$ and rms mass fluctuations on the scale of $8\,h^{-1}\,\text{Mpc}$ $\sigma_8 = 0.8$. The fiducial model we use is slightly away from the ΛCDM point in the DE parameter space: $\{w_0, w_a\} = \{-0.9, -0.24\}$, as fitted by Zhao & Zhang (2010) against a large number of available data. The transfer function for the scale dependence of matter density perturbations is calculated via the fitting formulae of Eisenstein & Hu (1998), which take the baryonic features in the matter power spectrum into account.

We use the redshift distribution of sources of the EMU and WODAN surveys (Fig. 1), as outlined in Sections 2.1–2.2. The median redshift of the survey is $z_m = 1.1$. The total number of

sources is 2.2×10^7, for EMU, and 7.3×10^6, for WODAN. The total sky coverage is 4π, three quarters coming from EMU and one quarter from WODAN. As pointed out above, we should have access to this overall redshift distribution beforehand.

8.1 No redshift information

First, we present the constraints that can be put on the cosmological parameters if no redshift information is available. The marginal errors σ_{φ_i} on the fiducial values μ_{φ_i} of the parameters φ_i, as well as the correlations between the parameters and w_0 or w_a, are shown in Table 3. The numbers in brackets refer to results including the full Fisher matrices for *Planck* and Union2. These marginal errors are approximately of the same order of magnitude as the parameter fiducial value. However, when we add CMB and SNeIa information, the forecast significantly improves. Nevertheless, it is still impossible to discriminate between the ΛCDM model and DE. This is because at the time of recombination the DE component was massively subdominant compared to matter and radiation, and the use of CMB is therefore not enough. Similarly, though they are a powerful probe for the late-time accelerated expansion of the cosmos, SNeIa are only sensitive to the background dynamics.

A possible solution to this problem is to include in the analysis information from other cosmological probes, as has been done by Raccanelli et al. (2012). Alternatively, we can investigate how much information is hidden in the redshift distribution of the radio sources detected by EMU and WODAN.

8.2 Full redshift information

Before showing the results obtained with the realistic strategy outlined in Section 4, we briefly discuss an extreme idealistic case for comparison. Here, we assume we perfectly know the redshifts of all the EMU and WODAN sources. Then, if we used the same bins of width 0.1 as shown in Fig. 1, we would have at our disposal 33 spectra combined into a tomographic matrix $C_{ij}^g(\ell)$. Each element of the matrix is a galaxy angular power spectrum as in equation (3), with the fraction of sources contained in the corresponding bin. It is worth noting that such a tomographic matrix is diagonal, since any cross-correlation between different bins vanishes. In other words, sources in the ith bin do not overlap in redshift with sources in the jth bin.

The marginal errors σ_{φ_i} on the fiducial values μ_{φ_i} of the parameters φ_i, as well as the correlations between the parameters and w_0 or w_a, are shown in Table 4. The numbers in brackets refer to the results including the full Fisher matrices for Planck and Union2.

In this extreme case, the results are unsurprisingly excellent. The possibility of binning the EMU and WODAN sources allows us to track the evolution of DE up to high redshifts, thanks to the long tail of the distribution of the radio sources (see Fig. 1). Indeed, even though DE is a subdominant species compared to matter until very late times, it is crucial to study its evolution, in order to constrain w_a. Moreover, the combination of both surveys yields a full-sky coverage, thus providing better statistics. As a result, the forecast marginal errors on the DE parameters are $\sigma_{w_0} = 0.022$ and $\sigma_{w_a} = 0.058$, which become $\sigma_{w_0} = 0.012$ and $\sigma_{w_a} = 0.033$ when combined with Planck and Union2. These constraints finally give FoMs of 1.9×10^3 and 5.4×10^3, respectively.

The correlation coefficients $r_{\varphi_i - w_0}$ and $r_{\varphi_i - w_a}$ are particularly useful to understand whether this present binning method is able of disentangling the parameter dependencies and lift some of their degeneracies. Indeed, if we look at the correlation coefficients in

---

[7] Note that indices α, $\beta = 1, \ldots, 8$ refer to the complete set of parameters ϑ, whilst $i, j = 1, \ldots, 6$ label the sub-set φ.

Table 3. Cosmological constraints when assuming no redshift information for the EMU/WODAN sources. Marginal errors σ_{φ_i} on the fiducial values μ_{φ_i} of the DE model parameters φ_i and their correlation with w_0 and w_a, viz. $r_{\varphi_i-w_0}$ and $r_{\varphi_i-w_a}$; σ_8 and b_{g} have been marginalized over. Numbers in brackets refer to the inclusion of Planck and Union2 Fisher matrices.

φ_i	μ_{φ_i}	σ_{φ_i}		$r_{\varphi_i-w_0}$		$r_{\varphi_i-w_a}$	
Ω_{m}	0.28	0.18	(0.00080)	0.78	(− 0.335)	−0.81	(0.20)
Ω_{b}	0.045	0.055	(0.0028)	0.535	(− 0.62)	−0.555	(0.63)
w_0	−0.9	2.47	(0.11)	1	(1)	−0.99	(− 0.985)
w_a	−0.24	9.60	(0.40)	−0.99	(− 0.985)	1	(1)
h	0.7	0.19	(0.00036)	0.026	(0.62)	−0.056	(− 0.62)
n_s	0.96	0.14	(0.0036)	−0.56	(− 0.06)	0.62	(0.19)

Table 4. The same as Table 3 for the unrealistic case where we have precise redshift information from all the sources of the survey.

φ_i	μ_{φ_i}	σ_{φ_i}		$r_{\varphi_i-w_0}$		$r_{\varphi_i-w_a}$	
Ω_{m}	0.28	0.004 25	(0.000 34)	0.48	(− 0.27)	−0.68	(0.059)
Ω_{b}	0.045	0.0013	(0.000 23)	0.43	(− 0.0076)	−0.61	(0.020)
w_0	−0.9	0.022	(0.012)	1	(1)	−0.92	(− 0.89)
w_a	−0.24	0.058	(0.033)	−0.92	(− 0.89)	1	(1)
h	0.7	0.0032	(0.000 029)	−0.044	(0.47)	−0.23	(− 0.145)
n_s	0.96	0.0057	(0.0021)	−0.18	(0.32)	0.46	(− 0.053)

Table 3, we find that some of them are near unity in absolute value. This means that these constraints are strongly degenerate with each other; this is because the closer to unity is the value of $r_{\varphi_i-\varphi_j}$, the more correlated are the two parameters φ_i and φ_j. On the other hand, the correlations obtained in combination with Planck and Union2 are far better for all the parameters.

8.3 Realistic binning strategy

Now, we present the realistic results that the procedure discussed in Section 4 will yield. Since we are now dealing with the cross-identified sources, their redshifts (and the relative error we have to assume) are dependent on the optical survey used for the cross-identification, as summarized in Table 2. The EMU radio sources will be identified by SkyMapper, which will provide photometric estimates for the source redshifts. Therefore, we divide the distribution $\mathrm{d}N/\mathrm{d}z(z)$ of Fig. 1 (red curve) into five bins up to $z = 0.8$ and assume a scatter $\sigma_z^{\mathrm{ph}} = 0.05(1 + z)$. For WODAN, the situation is slightly more complicated. This is because SDSS will provide spectroscopic measurements for objects with $z \lesssim 0.3$, whilst we will have to rely on photometric redshifts for the sources at higher redshift. Hence, in this case we subdivide the source distribution into three spectroscopic redshift bins of width 0.1 up to $z = 0.3$, plus three photometric redshift bins up to $z \simeq 0.8$. As described in Section 4, we then consider two more bins, but that do not correspond to a specific redshift: one for all the radio galaxies in the same sky area covered by SkyMapper/SDSS which are not cross-identified (case *ii* of the 'effective surveys') and another for all other radio galaxies in patches of the sky not covered by the redshift surveys (case *iii*).

Fig. 4 presents the 1σ confidence region in the (w_0, w_a)-plane as obtained by using the radio sources (black ellipse) and when we also add Planck and Union2 (red ellipse); for comparison, we also show the ellipse for Planck and Union2 alone (grey ellipse). The marginal errors σ_{φ_i} on the fiducial values μ_{φ_i} of the parameters φ_i, as well as the correlations between the parameters and w_0 or w_a, are shown in Table 5. Again, the numbers in brackets refer to results including the full Fisher matrices for Planck and Union2.
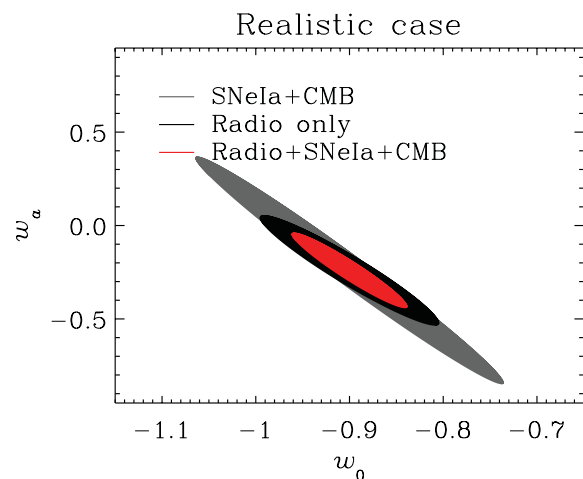
Figure 4. Marginal 1σ contour in the (w_0, w_a)-plane of the DE model for our realistic binning strategy. The black ellipse refers to the Fisher matrix obtained by using only EMU and WODAN galaxies and their cross-identifications with SkyMapper and SDSS, whilst the red ellipse includes Planck and Union2 priors; for comparison, the grey ellipse shows the contour for Planck and Union2 alone.

As expected, these results are not as tightly constraining as those obtained in the idealistic case of a perfect knowledge of all the source redshifts, but are a substantial improvement over the no-redshift case. Indeed, we obtain $\sigma_{w_0} = 0.063$ and $\sigma_{w_a} = 0.195$, which become $\sigma_{w_0} = 0.041$ and $\sigma_{w_a} = 0.13$ when combined with Planck and Union2. The correlation coefficients again help to obtain a deeper understanding of these results. As in the idealistic case, the tightness of the constraints on the parameters is fortified by the modest degeneracies yielded by our method. For this purpose, the inclusion of CMB and SNeIa priors is often crucial.

For instance, in Fig. 5 we show, for some of the cases scrutinized, the power spectra $C^{\mathrm{g}}(\ell)$ (solid, black) with the corresponding error

Table 5. The same as Table 3 for the realistic binning strategy.

| φ_i	μ_{φ_i}	σ_{φ_i}		$r_{\varphi_i - w_0}$		$r_{\varphi_i - w_a}$	
Ω_m	0.28	0.15	(0.000 56)	−0.76	(− 0.46)	−0.63	(0.20)
Ω_b	0.045	0.0067	(0.0011)	0.72	(− 0.34)	0.61	(0.26)
w_0	−0.9	0.063	(0.041)	1	(1)	0.96	(− 0.95)
w_a	−0.24	0.195	(0.13)	0.96	(− 0.95)	1	(1)
h	0.7	0.019	(0.00014)	0.16	(0.345)	0.12	(− 0.26)
n_s	0.96	0.011	(0.00295)	−0.83	(0.37)	−0.72	(− 0.17)

bars given by

$$\Delta C^g(\ell) = \sqrt{\frac{2}{(2\ell + 1) f_{sky}}} \left[C^g(\ell) + \frac{1}{N_g} \right], \qquad (16)$$

in comparison with a DE model whose $\{w_0, w_a\}$ values are 3σ away according to the errors quoted in Table 5 (dashed, red). Specifically, clockwise starting from the top-left panel: the power spectrum for the EMU+WODAN sources without redshift information; that for

the EMU+WODAN sources not cross-identified by either SkyMapper or SDSS; the $C^g(\ell)$ of the fifth, and last, photometric bin of the sources cross-identified by SkyMapper; and that of the first spectroscopic bin of the radio galaxies cross-identified by SDSS.

We can quantify how much our approach permits a discrimination between DE and ΛCDM by determining the FoMs. In our realistic case, the constraints on w_0 and w_a yield FoM = 382 or 225 for the radio sources with or without CMB and SNeIa, respectively. All these major results, together with the marginal errors on w_a and on the maximally constrained value of $w_{DE}(z) - w_p$ of equation (15) – are presented in Table 6.

Finally, we want to understand how the assumptions made upon the redshift evolution of the bias influence our results. To this aim (see Section 5.1) we make use of the additional nuisance parameter B_b, as in equation (5), thus introducing a further redshift dependence of the bias. We again perform the same Fisher analysis as before, where the set of nuisance parameter we want to marginalize over is now $\psi = \{\sigma_8, A_b, B_b\}$. As expected, the presence of one more free parameter leads to weaker constraining power. As a result, the
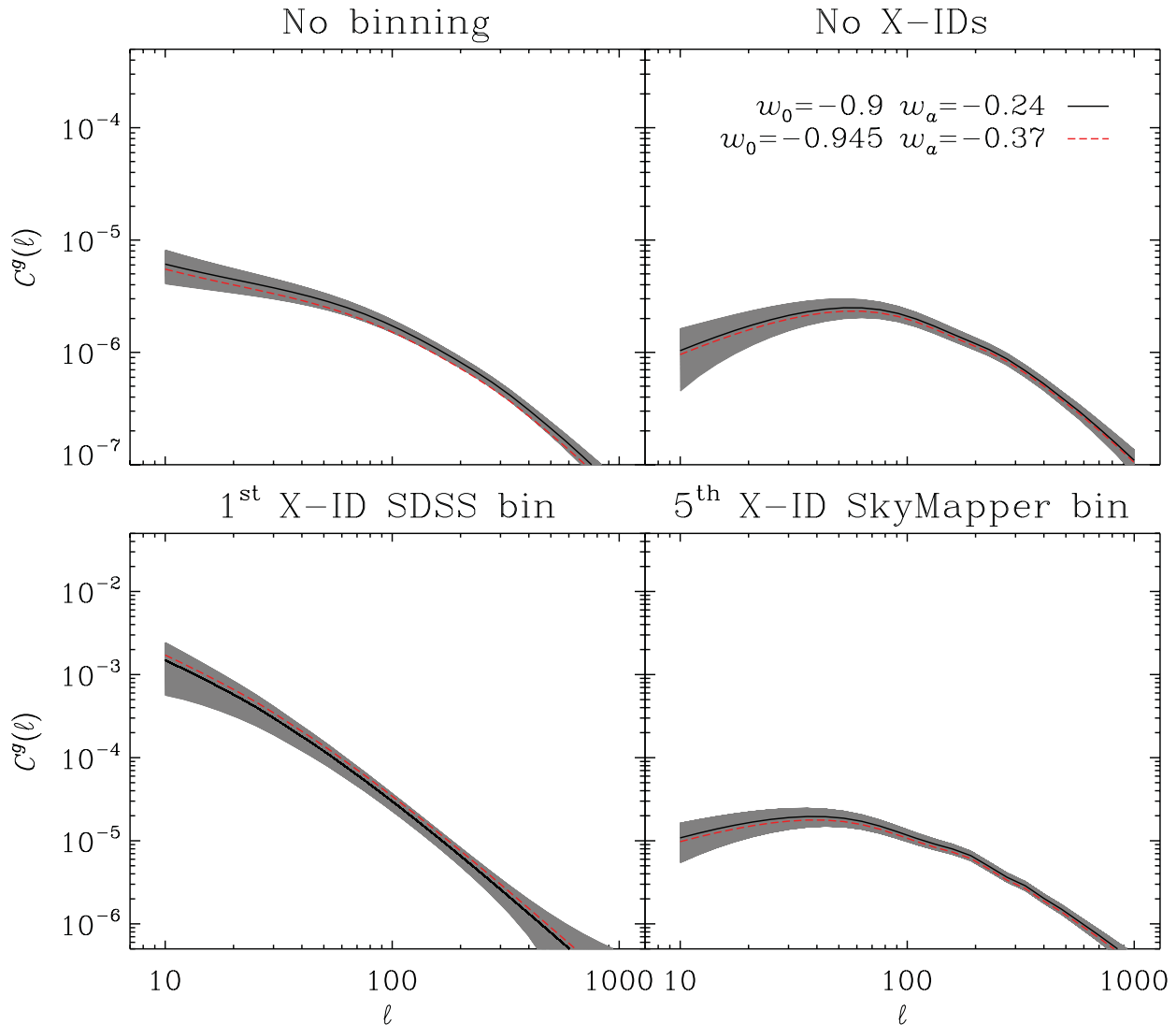
Figure 5. Comparison between the angular power spectra for the fiducial DE model (solid, black with error bars) and a DE cosmology with $\{w_0, w_a\}$ values 3σs away (dashed, red). Top-right panel: EMU+WODAN sources without any redshift information. Top-left panel: EMU+WODAN sources not cross-identified by SkyMapper or SDSS. Bottom-left panel: first spectro-z bin of the WODAN sources cross-identified by SDSS. Bottom-right panel: fifth (and last) photo-z bin of the EMU sources cross-identified by SkyMapper.

Table 6. Summary of the errors on w_0, w_p and w_a, and the FoMs for the unbinned, idealistic and realistic cases without (or with) Planck and Union2.

	No binning		Idealistic case		Realistic case	
σ_{w_0}	2.47	(0.11)	0.022	(0.012)	0.063	(0.041)
σ_{w_p}	0.29	(0.018)	0.0090	(0.0057)	0.020	(0.013)
σ_{w_a}	9.60	(0.40)	0.058	(0.033)	0.195	(0.13)
FoM	0.40	(140)	1909	(5378)	260	(603)
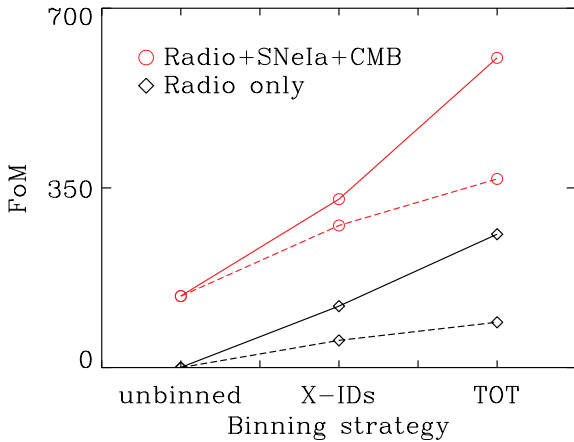
Figure 6. FoMs with or without the inclusion of Planck and Union2 (red circles or black diamonds, respectively) versus the binning strategy adopted: 'unbinned' pertains to the case with no redshift information, 'X-IDs' to the EMU/WODAN sources cross-identified by SkyMapper/SDSS and 'TOT' to the inclusion of all the effective surveys. Solid lines refer to the main case, whilst dashed lines to the case with an additional linear parametrization for the bias.

w_0–w_a ellipse is broader than in the realistic case. Nevertheless, we want to demonstrate that, even in this pessimistic case, our approach gives interesting results.

Therefore, to conclude, Fig. 6 summarizes the primary results of this work. It depicts the FoM versus the binning strategy adopted, thus showing the impact of our proposed pipeline. The labels of the horizontal axis refer to the unbinned case (unbinned), the case with cross-identified sources alone (X-IDs) and the case resulting from the combination of all the effective surveys (TOT) – (i)+(ii)+(iii) as explained in Section 4. Black diamonds refer to the use of only EMU and WODAN galaxies and their cross-identifications with SkyMapper and SDSS, whilst red circles point to the results obtained by the inclusion of the Fisher matrices for Planck and Union2. Solid lines refer to the main result for the realistic case, as highlighted in the previous section; dashed lines instead show what happens in the case just described of a two-parameter bias. It is clear that the inclusion of cross-identifications and, furthermore, the high-z radio tail still yields a significant enhancement.

9 SUMMARY AND CONCLUSIONS

In this paper, we have explored the impact that redshift information could have on the cosmological potential of the forthcoming generation of large-scale, radio continuum surveys. Specifically, we have investigated how the possibility of binning the redshift distribution of the radio sources would improve the constraining power of these surveys. For this purpose, as a fiducial model we adopted a dynamical DE model whose fiducial values have been fitted by

Zhao & Zhang (2010) as $\{w_0, w_a\} = \{-0.9, -0.24\}$. We have focused on two forthcoming wide-field radio surveys: EMU and WODAN. Thanks to their sensitivity and the specifics outlined in Table 1, they could be combined thus yielding a full-sky survey. This is extremely important, since it leads to larger sample size and allows us to lessen the impact of cosmic variance.

We have performed a Fisher matrix analysis to forecast how the combination of EMU and WODAN will be able to constrain the cosmological parameters of the DE model, particularly focusing on its extra parameters, w_0 and w_a, and using the angular power spectrum of radio sources as the cosmological probe. We have examined the impact of including redshifts for sources cross-identified with optical redshift surveys. We have described results when there is no knowledge of redshifts, summarized in Table 3; in this case the DE equation of state is poorly determined. We have also presented the most idealistic case where all the EMU and WODAN redshifts are known, in which case we have unsurprisingly obtained extremely tight constraints on all the model parameters, with marginal errors on the DE equation-of-state parameters $\sigma_{w_0} = 0.012$ and $\sigma_{w_a} = 0.033$, when combined with Planck and Union2.

Next, we moved to a more realistic scenario. We have included forthcoming optical surveys as cross-identifiers for the EMU/WODAN sources; specifically, we have used SkyMapper for the southern sky, while SDSS provides redshifts in the north. It is clear that not all of the radio galaxies that will be detected by EMU and WODAN will be cross-identified by other surveys, as these radio surveys cover the whole sky and reach very high redshift. To take this into account, we have developed a model of the future practical analysis, using three 'effective surveys' as described in Section 4. For these sub-surveys, the redshift distribution of sources will be those of: *(i)* all the EMU/WODAN galaxies cross-identified by SkyMapper/SDSS, suitably redshift binned; *(ii)* all the EMU/WODAN galaxies which are in the same patch of sky as SkyMapper/SDSS but which are not cross-matched and *(iii)* an EMU/WODAN survey probing only the sky left uncovered by SkyMapper/SDSS. With this approach we have obtained an FoM of 603 and 260 for the radio sources with and without CMB and SNeIa priors, respectively. These results are very competitive when compared with other surveys that will also be available in the near future. The improvement obtained by this cosmological analysis with radio surveys stems from the fact that by cross-correlating with shallow 'redshift surveys' we can make use of the long high-redshift tail of the non-identified radio galaxies to provide an extra handle on the evolution of DE. This effect can be clearly seen in Fig. 6, where the jump from the second to the third point is only due to the extra information from the radio surveys.

We want to emphasize that we have accounted for the source bias amplitude A_b by using a nuisance parameter which was allowed to vary freely. However, reality might be more complicated with effects on the bias such as scale dependence and a change in the relative amplitudes of the bias for each finer redshift bin. We leave a deeper analysis for future work. It is worth noting that the radio source bias could be constrained as a function of redshift by deep cross-correlation studies with optical data over smaller areas, but any remaining uncertainty requiring more bias parameters will worsen the FoMs. To simply test whether our approach is robust even in the presence of a more complex bias, we have also studied a slightly more complex scenario, in which we have added a linear correction to the bias amplitude. This means that we deal with one more nuisance parameter. Nevertheless, Fig. 6 shows that the main results of this work still hold, though the constraints get broader, as expected. On the other hand, if we parametrized the functional form

of the bias not only by its amplitude but also by taking its shape into account, we should be able to lift the strong degeneracy present here between A_b and the matter power spectrum normalization σ_8.

We have also not accounted for possible contaminants to the power spectrum that could affect our analysis, since the objective of this paper is to concentrate on the impact of redshift information for cosmological applications. In particular, double sources could affect the angular power spectrum at smaller angular scales ($< 0°.1$), requiring some cleaning technique (see e.g. Overzier et al. 2003, for the case with NVSS data). Note, however, that for the $10\sigma-10\,\mu\mathrm{Jy}$ flux cut we are considering here, these double sources should be much less abundant and much less dominant than for the NVSS case, so that the contamination might be less severe on these sub-degree scales; moreover, we are cutting off our analysis at $\ell_{max} = 1000$.

Besides, instrumental effects may also alter the clustering signal. For instance, Blake, Mauch & Sadler (2004b) have pointed out that, for angular separations around $\sim 0°.2$, there is an unexpected deficit in NVSS data, which is very likely an instrumental effect due to the shortest baseline used in the observations. Similarly, Blake & Wall (2002) have shown the risk in not properly considering and modelling gradients in the surface density. Indeed, such effects may significantly influence the imprint of the large-scale structure. This is because, if we tried to fit the data with a theoretical angular power spectrum which does not account for these systematics, we would reconstruct the systematic density gradients as well as the fluctuations due to clustering. However, such problems should arise with flux cuts $\gtrsim 10\,\mathrm{mJy}$ (see also Blake et al. 2004b; Blake, Ferreira & Borrill 2004a), thus leaving our analysis free of this problem. Nevertheless, we plan to return to the specific issue of contamination and cleaning of the cosmological signal in a future analysis.

As a final remark, we note that the optical surveys we have used for the cross-identifications should be available at approximately the same time as EMU and WODAN, around 2015. Therefore, we can see that future large-scale radio surveys can not only provide a different observational wavelength window for constraining the cosmological model, but also provide competitive DE constraints. Related to this, we aim to exploit such a successful method in a forthcoming paper to also test modified gravity models (Camera et al., in preparation).

ACKNOWLEDGMENTS

REFERENCES

Abbott T. et al., 2005, preprint (astro-ph/0510346)
Albrecht A. et al., 2009, preprint (arXiv:0901.0721)
Amanullah R. et al., 2010, ApJ., 716, 712
Amendola L., Tsujikawa S., 2010, Dark Energy: Theory and Observations. Cambridge Univ. Press, Cambridge
Bartelmann M., 2010, Rev. Mod. Phys., 82, 331
Benitez N., 2000, ApJ, 536, 571
Blake C., Wall J., 2002, MNRAS, 329, L37
Blake C., Ferreira P. G., Borrill J., 2004a, MNRAS, 351, 923
Blake C., Mauch T., Sadler E. M., 2004b, MNRAS, 347, 787
Bolzonella M., Miralles J.-M., Pello' R., 2000, A&A, 363, 476
Bonfield D. G., Sun Y., Davey N., Jarvis M. J., Abdalla F. B., Banerji M., Adams R. G., 2010, MNRAS, 405, 987
Chevallier M., Polarski D., 2001, Int. J. Mod. Phys., D10, 213
Collister A. A., Lahav O., 2004, Publ. Astron. Soc. Pac., 116, 345
Condon J. J., Cotton W. D., Greisen E. W., Yin Q. F., Perley R. A., Taylor G. B., Broderick J. J., 1998, AJ, 115, 1693
Cooray A., Sheth R. K., 2002, Phys. Rept., 372, 1
Eisenstein D. J., Hu W., 1998, ApJ, 496, 605
Eisenstein D. J. et al., 2011, AJ, 142, 72
Feldmann R. et al., 2006, MNRAS, 372, 565
Firth A. E., Lahav O., Somerville R. S., 2003, MNRAS, 339, 1195
Fisher R. A., 1935, J. R. Stat. Soc., 98, 39
Hu W., 2000, Phys. Rev. D, 62, 043007
Ilbert O. et al., 2006, A&A, 457, 841
Ivezic Z. et al., 2008, preprint (arXiv:0805.2366)
Jarvis M. J. et al., 2012, preprint (arXiv:1206.4263)
Johnston S. et al., 2008, Exp. Astron., 22, 151
Jungman G., Kamionkowski M., Kosowsky A., Spergel D. N., 1996, Phys. Rev. D, 54, 1332
Kaiser N., 1992, ApJ, 388, 272
Keller S. C. et al., 2007, Publ. Astron. Soc. Aust., 24, 1
Laureijs R. et al., 2011, ESA Definition Study Report, 12. ESA, Noordwijk
Lawrence A. et al., 2007, MNRAS, 379, 1599
Linder E. V., 2003, Phys. Rev. Lett., 90, 091301
McAlpine K., Smith D. J., Jarvis M. J., Bonfield D. G., Fleuren S., 2012, 423, 132
Norris R. P. et al., 2006, AJ, 132, 2409
Norris R. P. et al., 2011, Publ. Astron. Soc. Aust., in press (arXiv:1106.3219)
Oosterloo T., Verheijen M., van Cappellen W., 2010, PoS, ISKAF2010, 043
Overzier R., Rottgering H., Rengelink R., Wilman R., 2003, A&A, 405, 53
Peebles P. J. E., 1980, The Large-scale Structure of the Universe. Princeton Univ. Press, Princeton, NJ
Planck Collaboration, 2005, ESA-SCI, 1
Raccanelli A. et al., 2012, MNRAS, 424, 801
Rottgering H., 2003, New Astron. Rev., 47, 405
Rottgering H. et al., 2011, J. Astrophys. Astron. (arXiv:1107.1606)
Salvato M. et al., 2011, ApJ, 742, 61
Schinnerer E. et al., 2010, ApJS, 188, 384
Simpson C. et al., 2006, MNRAS, 372, 741
Tegmark M., Taylor A., Heavens A., 1997, ApJ, 480, 22
Wang Y., 2008, Phys. Rev., D77, 123525
Way M. J., Srivastava A., 2006, ApJ, 647, 102
Wilman R. et al., 2008, MNRAS, 388, 1335
Wilman R., Jarvis M., Mauch T., Rawlings S., Hickey S., 2010, MNRAS, 405, 447
Wright E. L. et al., 2010, AJ, 140, 1868
Zhao G.-B., Zhang X.-M., 2010, Phys. Rev., D81, 043518

This paper has been typeset from a TeX/LaTeX file prepared by the author.